4 RESULTS

4.1 Results 1

Neurons are polarized cells whose functions depend on the correct sorting and segregation of different proteins in different membrane microdomains. Cholesterol as a central component of synaptic DRMs has been shown to be essential for the maintenance of synapses (Hering, Lin et al. 2003), embryogenesis (Wolf 1999), and synaptogenesis (Nagler, Mauch et al. 2001; Mauch, Nagler et al. 2001). Compared with the function of postsynaptic DRMs to maintain dendritic spins and surface AMPA receptor stability (Hering, Lin et al. 2003), the role of presynaptic DRMs is unclear.

We used systematic quantitative tandem mass spectrometry combined with biochemical approaches to address the function of synaptic DRMs as a cargo sorting platform for synaptic cycling.

4.1.1 Flotillin 1 is localized in synaptic DRMs in a cholesterol dependent manner.

DRMs contain high concentration of cholesterol and sphingolipids. When cold nonionic detergents are used to solubilize biological samples, DRMs cannot be solubilized due to their high concentration of lipids. These non-extracted DRMs can be further purified from soluble fractions in sucrose gradients where buoyant DRMs float up to the top and soluble materials stay in the bottom fraction. Proteins in different fractions can be analyzed by Western Blot.

To optimize our conditions for synaptic DRM isolation, flotillin 1, a widely used marker for DRMs (Salzer and Prohaska 2001), was used to evaluate our experimental conditions. As shown in the upper panel (mock) of **Figure 4-1 A**, a clear peak of flotillin 1 was localized in the second fraction of the gradient, although the majority of the signal was in the bottom soluble fractions. This may due to the high ratio of detergent to protein which confers a more stringent isolation of DRMs. Instead, the transferrin receptor a non-raft protein was not detected in fraction two and was found exclusively in bottom fractions.

A general concern about biochemically-purified DRMs is that non-specific, i.e. cytoskeletal proteins might co-migrate to the light DRMs fraction in the gradient centrifugation. To avoid such false positive results, a control experiment for the identification of authentic DRMs

proteins was designed. Cholesterol is a basic component of DRMs. Depletion of cholesterol with drugs such as filipin (Geyer and Bornig 1975) or methyl-β-cyclodextran (MβCD) (Christian, Haynes et al. 1997) can dissociate DRMs structures. When DRMs were prepared from synaptosomes pretreated with 10 mM MβCD (**Figure 4-1 A** bottom panel), the DRM marker flotillin 1 was completely absent from the DRM-containing floating fraction and detected only in the bottom soluble fractions. Free cholesterol was depleted by ~90% under these conditions (**Figure 4-1 B**) as determined by a fluorometric assay using Amplex Red reagent. Based on the initial experiments, we define fraction #2 as the main DRM fraction.

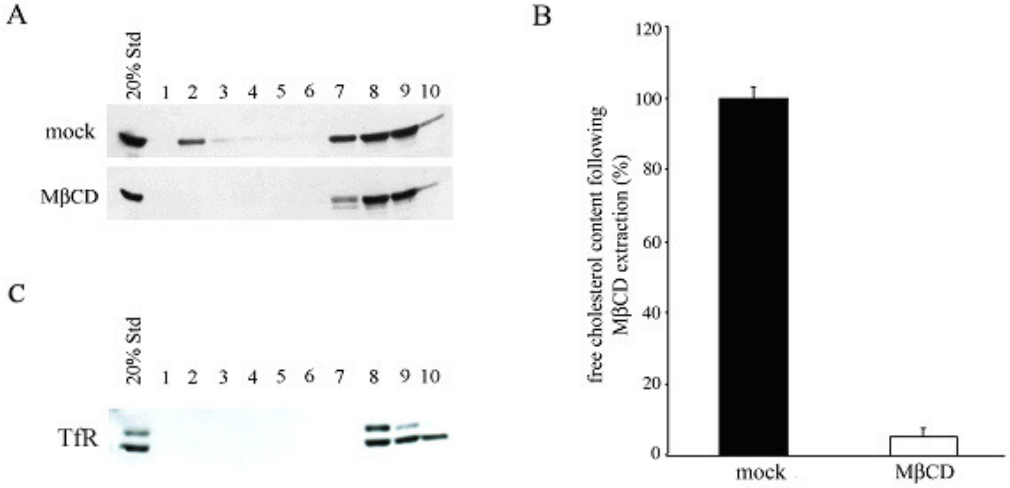

Figure 4-1 Flotillin 1 is localized to synaptic DRM fractions in a cholesterol-dependent manner

(A) Immunoblot analysis of fractions obtained from flotation gradients of Triton X-100-treated purified synaptosomes that had been extracted with methyl-β-cyclodextrin (MβCD) or mock-treated. 20% Std, 1/5 of the total material loaded at the bottom of the gradient. Flotillin 1 showed a peak signal in the DRM fraction # 2 (A, upper panel) which disappeared upon cholesterol depletion (A, lower panel).
(B) Cholesterol concentration determination indicated that >90% of free cholesterol had been depleted under these conditions.
(C) Experimental procedures were the same as that of the Mock from (A). Different fractions from up to bottom were blotted with TfR (transferrrin receptor)

4.1.2 Quantitative nanoLC-MALDI-MS/MS protomics reveals many synaptic vesicle and synaptic vesicle cycling proteins in synaptic DRMs

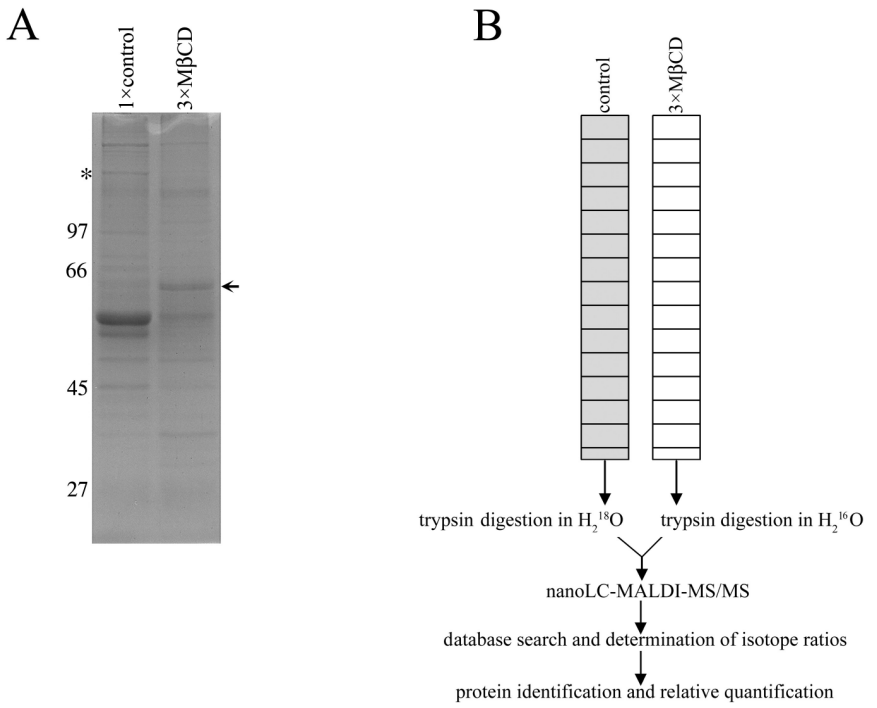

Figure 4-2 Sample preparation and working scheme for nanoLC-MALDI-MS/ MS

(A) Coomassie Blue-stained SDS-PAGE of floating DRM gradient fractions (fraction #2 in **Figure 4-1 A**) obtained from either mock-treated or cholesterol-depleted (MβCD) synaptosomal lysates. To ensure identification of protein bands in the MβCD-treated sample a 3-fold excess of material compared to control conditions was analyzed. Some bands (example highlighted by asterisk) completely disappeared, while others (example marked by arrow) remained unchanged after correcting for differential protein content.
(B) Schematic description of the experimental protocol used for quantitative NanoLC-MALDI-MS/MS identification of proteins.

Although many individual proteins have been shown to localize to DRMs, a systematic quantitative identification of DRMs proteins will provide important insights into the potential function of DRMs at synapses. The protein profile of DRMs in Hela cells has been determined by quantitative mass spectrometry analysis (Foster, De Hoog et al. 2003). We then took advantage of a similar approach involving isotope labeling during tryptic proteolysis combined with nanoLC-MALDI-MS/MS. DRM fractions (corresponding to fraction 2 in **Figure 4-1**) derived from mock- or MβCD-treated (3-fold excess to ensure unequivocal later identification by MS/MS) samples were resolved side-by-side using one-dimentional SDS-PAGE followed by staining with Coomassie Blue (**Figure 4-1 A**). Horizontally taken gel slices from each sample were then subjected to in-gel tryptic digestion in the presence of $H^{16}O$ (MβCD-treated sample) or $H^{18}O$ (control sample), samples were

mixed and finally analyzed by nano-LC-MALDI-MS/MS. The prior isotope encoding allows assignment of specific quantitative changes of only the cholesterol-dependent proteins in the DRM fraction (Foster, De Hoog et al. 2003). A schematic illustration of the experimental protocol is illustrated in **Figure 4-2 B**.

The $^{18}O/^{16}O$ ratios used for classification of DRM, DRM-associated and non-DRM proteins were modified from Foster *et al* (Foster, De Hoog et al. 2003). $^{18}O/^{16}O<3$, $3\leq{}^{18}O/^{16}O<6$, $^{18}O/^{16}O \geq 6$ were classified to be non-DRM, DRM-associated and DRM proteins, respectively. Totally, 159 proteins (supplementary table 1) were quantified of which 122 belonged to DRM or DRM-associated proteins. The comparison of isotopic distribution patterns of a DRM protein, the vacuolar proton pump (V-ATPase), and a non-DRM protein, 2-oxoglutarate carrier protein is shown in **Figure 4-3**.

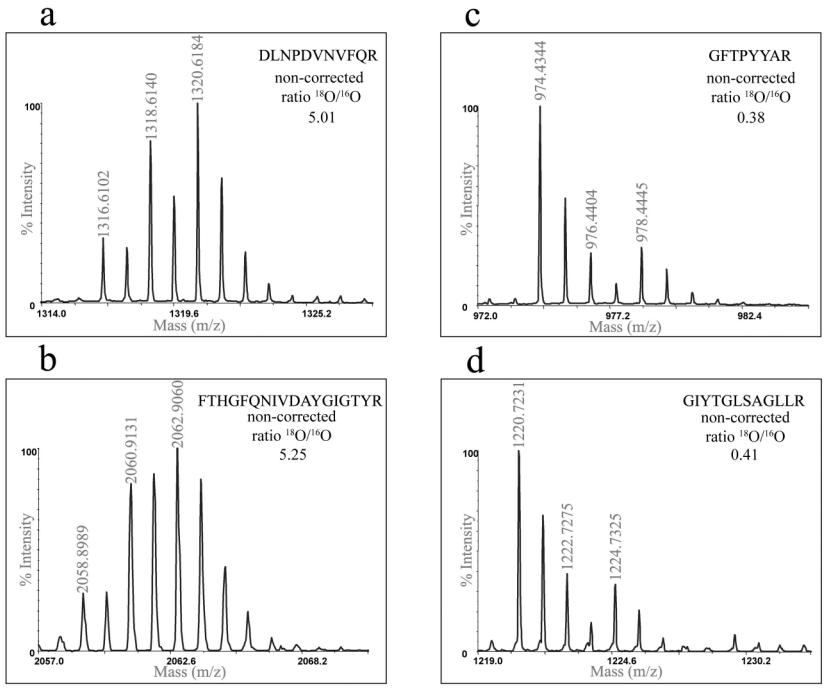

Figure 4-3 Comparison of isotopic distribution patterns obtained from a DRM protein

Vacuolar proton pump (V-ATPase), a non-DRM protein, and 2-oxoglutarate carrier protein were chosen to represent DRMs protein and non-DRMs protein, respectively. Two sequenced peptides from the V-ATPase, DLNPDVNVFQR and FTHGFQNIVDAYGIGTYR with corresponding masses of 1316.6102 and 2058.8989, respectively (a, b), displayed similar normalized $^{18}O/^{16}O$ ratios of 15.03 and 15.75, indicating a dramatic decrease of the V-ATPase in the DRM fraction upon cholesterol depletion. In contrast, two peptides GFTPYYAR and GIYTGLSAGLLR from the non-DRM protein 2-oxoglutarate carrier protein (c, d) showed $^{18}O/^{16}O$ ratios of 1.14 and 1.23, suggesting that they were not affected by the cholesterol content of the synaptic membrane. The sequenced peptides and the corresponding normalized $^{18}O/^{16}O$ ratios are indicated at the upper-right corners of each rectangle

Interestingly, among the polypeptides identified as DRM or DRM-associated proteins we found a variety of *bona fide* synaptic vesicle proteins including syanaptotagmin 1, synaptobrevin 2, synaptic proteins 2 (SV2), synapsin, Rab3 and V-ATPase. The

glycosylphosphatidylinositol-linked “raft” marker protein Thy-1 here identified as a component of synaptic DRMs has also been shown to be a common synaptic vesicle protein (Jeng, McCarroll et al. 1998). Proteins needed for exocytosis such as Munc18-1, SNAP-25a, NSF (N-ethylmaleimide sensitive factor) and for endocytic process including clathrin (heavy and light chains), AP-2, neuronal AP-3B (Galli and Haucke 2004), ATPase Hsc70 for uncoating (Chappell, Welch et al. 1986) and large GTPase dynamin for coat fission were identified to be DRM proteins (**Table 1**). Many of these factors have previously been shown to associate with cholesterol-rich membrane sites (*i.e*. SNAP-25, clathrin, and synaptobrevin 2) (Chamberlain, Burgoyne et al. 2001; Lang, Bruns et al. 2001), to directly bind cholesterol (*i.e*. synaptotagin 1 and synaptophysin) (Thiele, Hannah et al. 2000) or to form cholesterol dependent protein complexes i.e. synatophysin-synaptpbrevin 2 (Mitter, Reisinger et al. 2003; Galli, McPherson et al. 1996). Syntaxin1 can form a SDS-resistant SNARE complex with synaptobrevin 2 and SNAP-25. The missing identification of syntaxin 1 represents a possible sensitivity limitation of the used method. This was also true for flotillin 1 and PIPKIγ, although they were clearly identified to be associated with synaptic DRMs by immunoblots. Combination of two different tandem mass spectrometry methods may give more promising results.

DRMs have been implicated to be involved in the controlling of many cellular signal transduction and protein or lipid sorting processes. As expected, we could validate many of such proteins in synaptic DRMs such as $G\alpha_o$, $G\alpha_z$, $G\alpha_i$, $G\beta_1$, cGMP and cAMP phosphodiesterases, protein kinase C (β and γ) (Becart, Setterblad et al. 2003), prion protein (Taylor and Hooper 2006), calcium-calmodulin-dependent calcium channels, and the NR1 subunit of *N*-methyl-D-aspartate receptors (supplemental table). We also identified synaptic scaffolding molecules including PSD95 (postsynaptic density protein 95) (Wong and Schlichter 2004), PSD93, densin180, ProSAP/Shank2, Vesl-1L, SynGAP-a (a PSD-95-binding Ras-GAP), tubulin (Li, Shaw et al. 2004), 14-3-3 (γ and ζ), GAP-43, and septins 5 and 7 as well as the lipid-anchored proteins neurotrimin and paralemmin with DRMs. Surprisingly, mitochondria proteins especially F_0F_1-ATP-synthase were identified to be DRM or DRM-associated proteins. This is either a confirmation of the previous results showing that oxidation-reduction respiratory chains and ATP synthase were localized in cell surface lipid raft domains (Bae, Kim et al. 2004; Kim, Lee et al. 2006) or just a fractionation contamination of mitochondria enrichment in synaptosomes.

Table 1 DRM- or DRM-associated proteins involved in synaptic vesicle cycling identified and quantified by nanoLC-MALDI-MS/MS

Synaptic vesicle proteins			
Protein Name	**MW (Da)**	**Peptides MS/MS**	**Peptides used for quantification**
Rab3a	24954	3	YADDSFTPAFVSTVGIDFK LQIWDTAGQER
synaptic vesicle glycoprotein 2a (SV2a)	82608	4	QVHDTNMR GLDRVQDEYSRR
synaptobrevin 2 (VAMP 2)	12683	2	LQQTQAQVDEVVDIMR ADALQAGASQFETSAAK
synaptophysin	33289	3	MATDPENIIK MDVVNQLVAGGQFR
synapsin I	73943	10	QTTAAAAATFSEQVGGGSGGAGR MGHAHSGMGK
synapsin II	63417	5	SQSLTNAFSFSESSFFR QTAASAGLVDAPAPSAASR
synaptotagmin I	47441	2	VFVGYNSTGAELR VPYSELGGK
Thy-1 antigen	18160	3	VNLFSDR SRVNLFSDR
V-ATPase, V0 subunit A isoform 1	96265	6	SVFIIFFQGDQLK FLPFSFEHIR
V-ATPase, V1 subunit C, isoform 1	43873	2	TEFWLISAPGEK AVDDFRHK
V-ATPase, V0 subunit D isoform 1	51010	9	NVADYYPEYK FFEHEVK
V-ATPase, V1 subunit A, isoform 1	68222	16	ADYAQLLEDMQNAFR IKADYAQLLEDMQNAFR
V- ATPase subunit E1	26112	3	IMEYYEKK IMEYYEK
Exo- and endocytotic proteins			
adaptor protein complex AP-2, alpha subunit	103979	3	YGGTFQNVSVK AVEYLR
adaptor protein complex AP-2, beta 2 subunit	105691	2	ALQHMTDFAIQFNK LASQANIAQVLAELK
adaptor protein complex AP-3, beta3B subunit	119096	3	ATGYQELPDWPEEAPDPSVR EFQTYIR
clathrin, heavy chain	191477	7	VANVELYYK SVNESLNNLFITEEDYQALR
clathrin light chain	26964	3	VADEAFYK ELEEWYARQDEQLQK
dynamin 1	95867	11	TGLFTPDLAFEATVK RSPTSSPTPQR
Hsc70	70884	18	IINEPTAAAIAYGLDKK NSLESYAFNMK
Munc18-1	67568	3	REPLPSLEAVYLITPSEK VLVVDQLSMR
N-ethylmaleimide sensitive fusion protein (NSF)	82600	8	VVNGPEILNKYVGESEANIR KLFADAEEEQR
SNAP-25a	20545	5	AWGNNQDGVVASQPAR ADQLADESLESTRR
SNAP-25-interacting protein	129665	9	HTQGAQPGLADQAAK SLVGFGPPVPAKDTETR

All proteins except synaptophysin exhibited $^{18}O/^{16}O$ ratios > 6

We have grouped the 122 identified DRM and DRM-associated proteins into several families depending on their known and presumed functions (**Figure 4-4**).

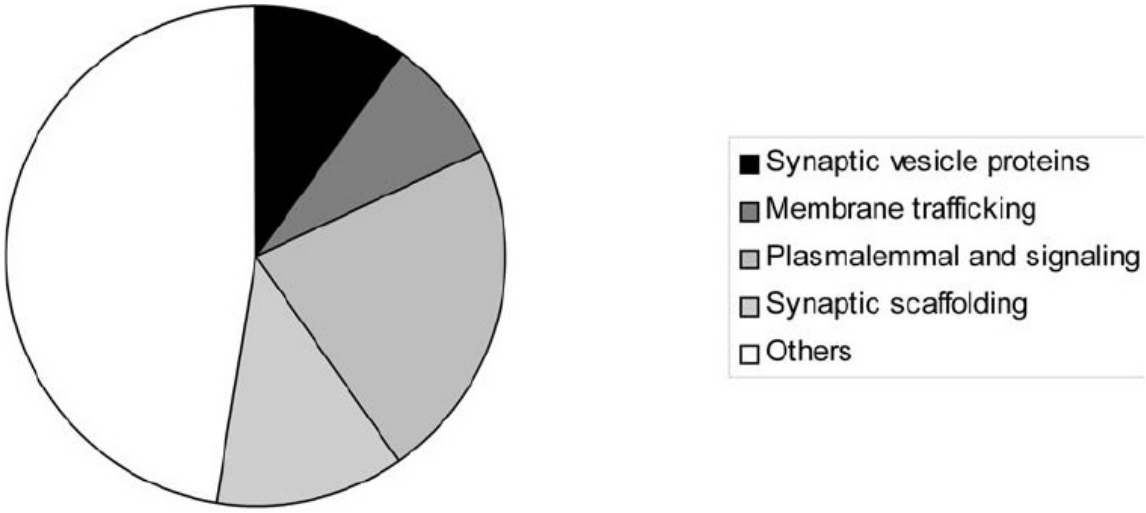

Figure 4-4 Synaptic DRMs and DRM-associated proteins reveal diverse cellular functions

122 proteins were grouped into different classes according to their known and presumed functions. The relative enrichment is shown in this pie explosion.

4.1.3 Confirmation of DRMs localization of some synaptic vesicle and endocytic proteins by immunoblotting

To confirm the cholesterol-dependent localization of some interesting proteins, same experimental procedures were used as for the quantitative proteomics analysis but instead detected by immunoblot. The selected top three fractions and one bottom fraction, either No.8 (**Figure 4-5 B** and **C**) or 1/of bottom 4 (**Figure 4-5 A**) fractions from totally 10 fractions are shown here. Synaptic vesicle proteins synaptotagmin 1, synaptobrevin 2 and synaptophysin were all detected in No.2 buoyant DRMs that were dependent on the presence of cholesterol using Trition X-100 as detergent. The endocytic proteins clathrin and AP-2 showed a similar distribution pattern as to flotillin 1 in **Figure 4-1 A**. Morever, we could detect small amounts of PIPKIγ in synaptic DRMs, suggesting that $PI(4,5)P_2$ synthesis may at least in part occur within cholesterol-rich membrane sites (Pike and Miller 1998). PIPKIγ was not identified in the quantitative proteomic analysis probably due to its low abundance. Its kinase activity could be stimulated by a small GTPase Arf6 in synapse and as a result, the locally-generated $PI(4,5)P_2$ on PM could serve as a hotspot for recruitment of clathrin and AP-2 (Krauss, Kinuta et al. 2003).

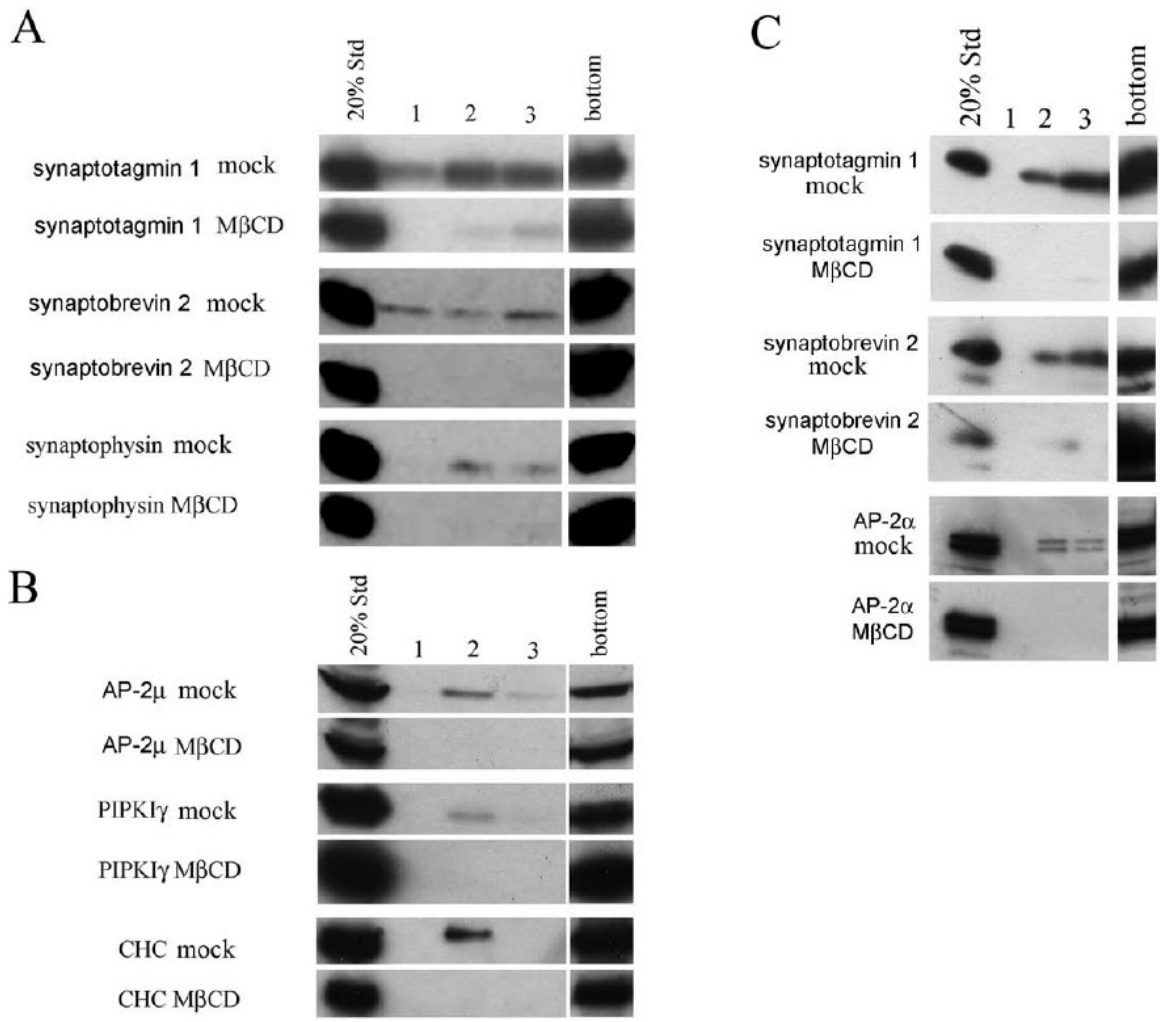

Figure 4-5 Some synaptic vesicle and endocytic proteins are localized to synaptic DRM fractions

(A) Immunoblot analysis of the distribution of the synaptic vesicle proteins synaptotagmin 1, synaptobrevin 2, and synaptophysin within DRM (#1-3) and non-DRM fractions (bottom) isolated from flotation gradients after mock or MβCD treatment of Triton X-100-lysed synaptosomes.
(B) Immunoblot analysis of the distribution of the endocytic proteins clathrin (CHC), AP-2μ, or phosphatidylinositol 4-phosphate 5-kinase type Iγ (PIPKIγ) within DRM (#1-3) and non-DRM (bottom) fractions isolated from flotation gradients after mock or MβCD treatment of Triton X-100-lysed synaptosomes.
(C) Distribution of synaptotagmin 1, synaptobrevin 2, and AP-2α within DRM (#1-3) and non-DRM (bottom) fractions isolated from flotation gradients after mock or MβCD treatment of CHAPS-lysed synaptosomes.

Triton might promote artificial aggregration (Heerklotz 2002). To test whether the synaptic DRM localization of synaptic vesicle and endocytic proteins was caused by the use of Triton X-100, the same experimental parameters were used except using CHAPS instead of Triton X-100. Immunoblot results showed that synaptotagmin 1, synaptobrevin 2 and AP-2 had a similar cholesterol-dependent synaptic DRM localization pattern compared with experiments using Trition X-100, which demonstrated that these proteins' distribution at PM DRMs may be only a reflection of their intrinsic property instead of artefacts caused by using certain detergent *in vitro*.

4.1.4 A cholesterol-dependent synaptic vesicle complex containing synaptotagmin 1, synaptobrevin 2 and synaptophysin

We have found that many synaptic vesicle, exo- and endocytic cycling proteins are localized in synaptic DRMs. If vesicle proteins are really kept as an entity in DRMs during synaptic vesicle cycling, the depletion of cholesterol could disturb this recycling process. Synaptophysin is a cholesterol binding protein (Thiele, Hannah et al. 2000) and forms a Triton resistant complex with synaptobrevin 2 in a cholesterol dependent manner to regulate the formation of SNARE complex and thereby modulates synaptic efficiency (Mitter, Reisinger et al. 2003). Due to the high cholesterol content in synaptic vesicle, we speculate that synaptic vesicle proteins may form complexes. Using zwitterionic CHAPS to extract crude synaptic vesicles, we found that synaptotagmin 1 could precipitate synaptophysin, synaptobrevin 2 and SV2 but not non-DRM synaptic vesicle protein synaptogyrin (**Figure 4-6 A**). Cholesterol-depletion dramatically decreases the precipitated synaptophysin and synaptobrevin 2 to about 20% and 50%, respectively; instead the SV2 signal does not change much (**Figure 4-6 C**). This result is consistant with the previous observation indicating a direct interaction of both proteins (Schivell, Mochida et al. 2005). γ-glutamic acid decarboxylase 6 (GAD6), as a control, did not precipitate all the proteins detected in the synaptotagmin 1 co-immunoprecipitation experiment (**Figure 4-6 A**). The non-DRM transmembrane protein transferrin receptor does not recovery any of the three synaptic vesicle proteins (**Figure 4-6 B**), which excludes the possibility of an artefact transmembrane protein complex formation due to the detergent CHAPS. In this condition, cholesterol was depleted more than 80% as shown in **Figure 4-6 D**.

This cholesterol dependent complex formation is simply not an artefact due to any specific character of synaptotagmin 1 antibody used, since we could show a similar complex formation using antibodies against synaptophysin and synaptobrevin 2 as shown in **Figure 4-7**.

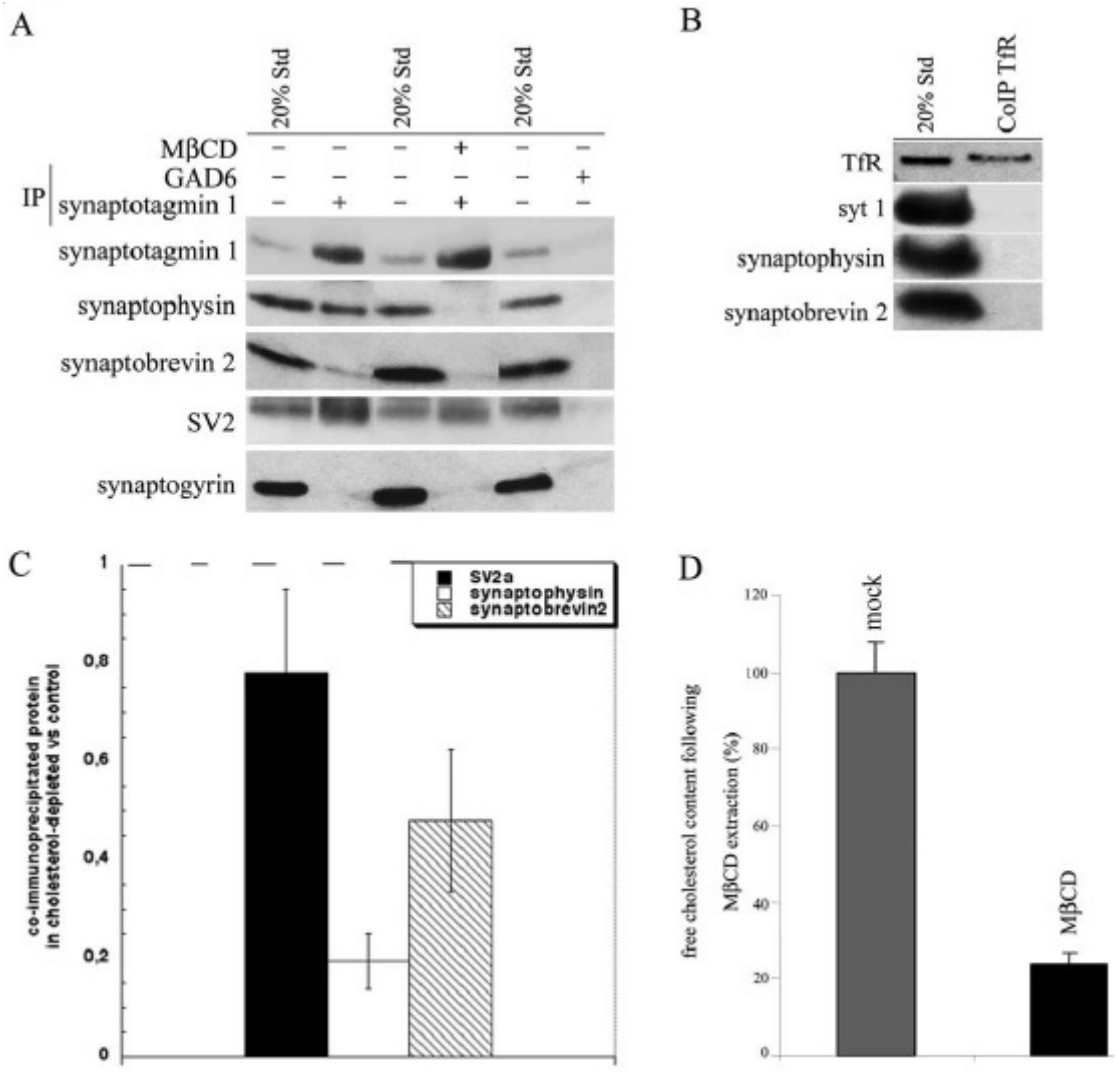

Figure 4-6 Synaptotagmin 1 forms a cholesterol-dependent protein complex with synaptophysin, and synaptobrevin 2

(A) Synaptotagmin 1 was immunoprecipitated from CHAPS-solubilized synaptic vesicle fractions (LP2) or cholesterol-depleted LP2 controls. Following extensive washes samples were analyzed by SDS-PAGE and immunoblotting. In addition to synaptotagmin 1 synaptophysin and synaptobrevin 2 were also found in the immunoprecipitate. Synaptogyrin, a non-DRM SV protein was not associated with this complex. All these proteins were absent from control precipitates using antibodies against γ-glutamic acid decarboxylase (GAD6) or the transferrin receptor **(B)**. Following MβCD-mediated depletion of cholesterol by 80% (mean ±SD; n=3) **(D)** the amounts of synaptophysin and synaptobrevin 2 associated with synaptotagmin 1 were reduced by about 80% or 50%, respectively. Quantitative immunoblots were developed with ^{125}I-protein A and analyzed by phosphoimage analysis. **(C)** Quantitative analysis of the amount of synaptophysin and synaptobrevin 2 associated with synaptotagmin 1. Data represent normalized mean (±SE; n= 3).

Using cold Triton X-100 extracted crude synaptic vesicles as starting materials; we could only detect a kind of sub-complex formation between synatophysin and synaptobrevin 2, which indicated that the supra-complex formation between synaptotagmin 1, synaptophysin, synaptobrevin 2 and possibly other synaptic vesicle proteins is just a weak non-covalent interaction due to the ability of cholesterol as a “glue”.

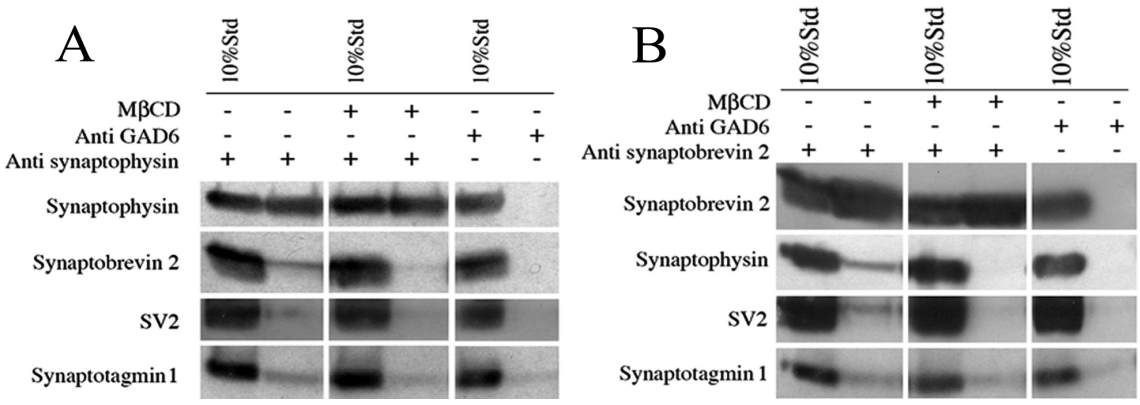

Figure 4-7 Cholesterol-dependent synaptic vesicle protein complex formation using antibodies against synpatophysin (A) and synaptobrevin 2 (B) for co-immunoprecipitation

Experimental procedures were the same as that of **Figure 4-6 A**, except that specific monoclonal antibodies against synptophysin (A) and synaptobrevin 2 (B) were used for CoIP. In both figures, synaptotagmin 1 signal was not decreased dramatically compared to that of synaptophysin possibly due to the sticky property of this protein.

4.1.5 Synaptic vesicle and endocytic proteins are partially resistant to Triton X-100 extraction in the cold in primary hippocampal neurons

Although some evidence supports the existence of lipid rafts *in vivo*, most studies are still based on the biochemical character of light buoyancy to isolate DRMs operationally *in vitro*. The dispute comes from the potential artefact induced by using cold nonionic detergent, which promotes the formation of big patches of PM from relatively small, heterogeneous domains (Heerklotz 2002). To avoid the complicated steps of biochemical isolation of DRMs, we used the primary hippocampal neurons to study the localization of synaptic DRM proteins *in situ*. Rat primary neuron-glia co-cultures (14-20 DIV) were washed with cold PBS or pre-warmed PBS and then treated with 0.5% Triton X-100 in 20 mM Na-Phosphate pH 7.4 for 10 min on ice or at 37°C, respectively. After residues of Triton X-100 were washed away, cells were fixed and processed to immunostaining. In control experiments, synaptobrevin 2 co-localizes with synaptophysin and synaptotagmin 1 (**Figure 4-8 A a** and **d**) in synaptic bouton with a puncta staining pattern, whereas non-DRM protein transferrin receptors mainly localize at somatodendritic compartments (**Figure 4-8 B**). After cold Triton X-100 extraction for 10 min, synaptic vesicle proteins are still localized in puncta (**Figure 4-8 b** and **e**). However, transferrin receptors are completely solubilized and no signal can be detected (**Figure 4-8 B h**). 37°C Triton X-100 extractions abolish all synaptic vesicle protein signals (**Figure 4-8 A c** and **f**).

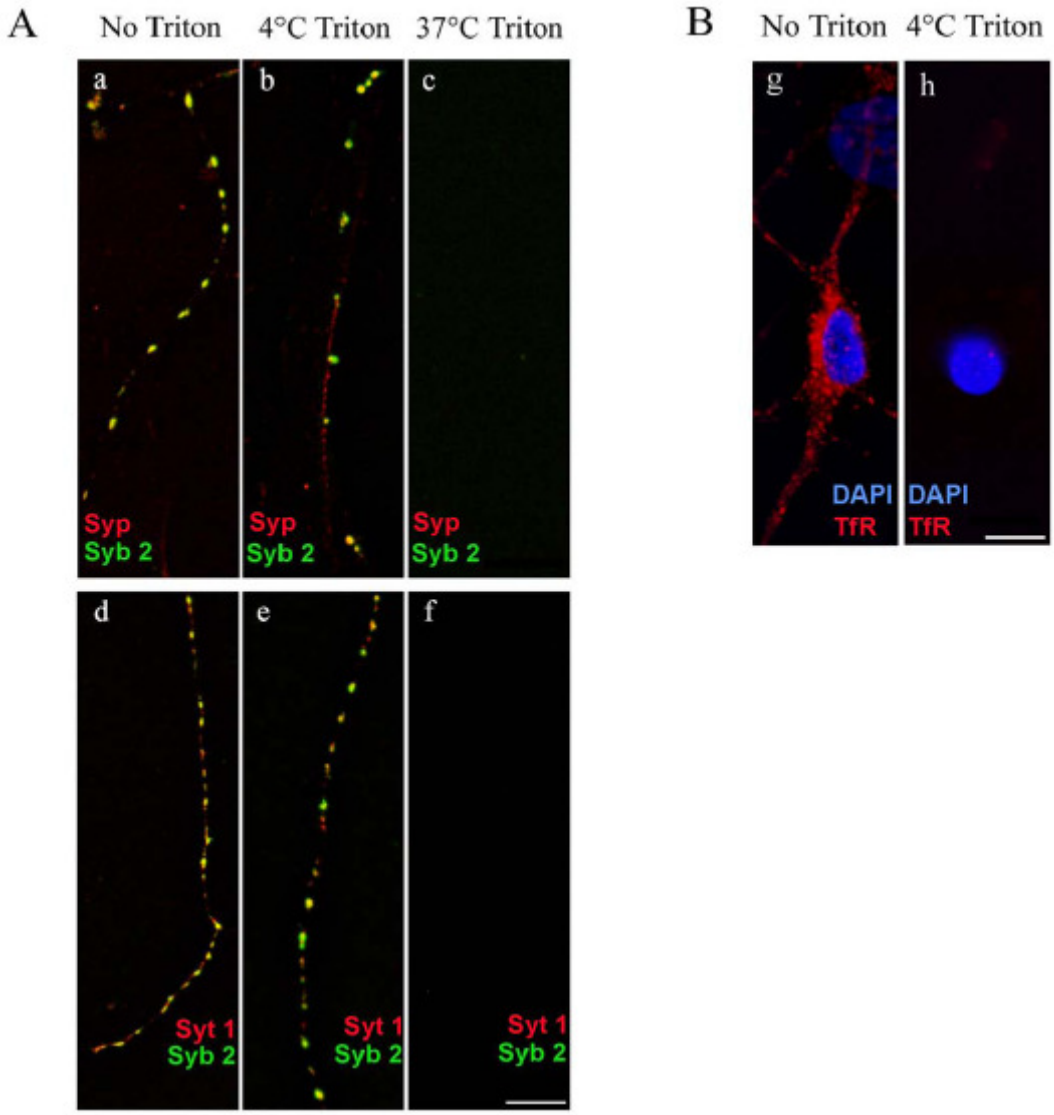

Figure 4-8 Synaptic vesicle proteins are partly resistant to extraction with Triton X-100 in hippocampal neurons

Hippocampal neurons isolated from newborn rats (14-20 DIV) were either left un-treated or extracted with Triton X-100 as indicated (see materials & methods). **(A)** Co-localization of synaptophysin (Syp, red), synaptobrevin 2 (Syb 2, green), and synaptotagmin 1 (Syt 1, red) under control conditions (a,d), or following extraction with 0.5% Triton X-100 at 4°C (b,e). Incubation with Triton X-100 at 37°C leads to complete solubilization (c,f). Merged images are shown. **(B)** By contrast, transferrin receptor (TfR, red) is completely solubilized and removed by extraction with 0.5% Triton X-100 at 4°C (compare g and h). DAPI (blue) staining is depicted for comparison. Scale bar, 10 µm.

The endocytic proteins clathrin and AP-2 also partially co-localize with synaptobrevin 2 in mock experiments (**Figure 4-9 A and C**). The co-localized signal is resistant to cold-Triton X-100 extractions as shown in **Figure 4-9 B and D**.

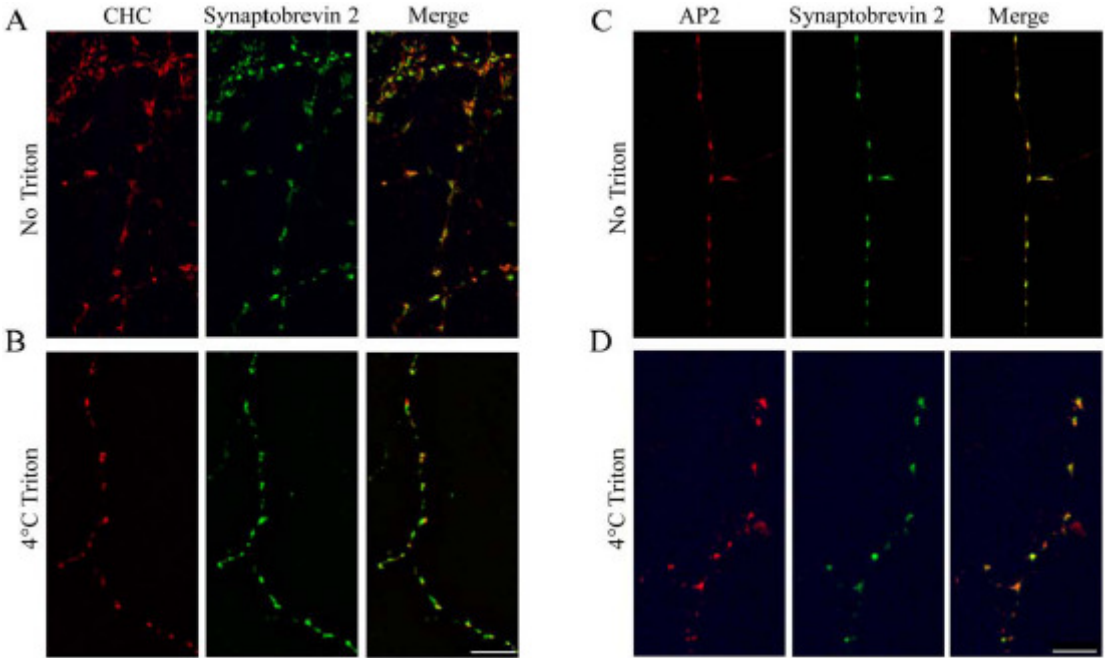

Figure 4-9 The endocytic proteins clathrin and AP-2 co-localize with synaptobrevin 2 in Triton X-100-extracted hippocampal neurons

The experiment was done as described in the legend to **Figure 4-8**. Clathrin **(A, B)** and AP-2 **(C, D)** both co-localize with synaptobrevin 2 in mock-treated or Triton X-100-extracted (4°C) hippocampal neurons. Following incubation with Triton X-100 at 37°C clathrin and AP-2 were completely solubilized together with synaptobrevin 2 (data not shown). Scale bar, 10 µm.

4.1.6 Synaptic vesicle proteins co-localize with FITC-labeled cholera toxin B in stimulated primary neurons

Treatment of hippocampal neurons with detergent is a relatively harsh method to assign localization of proteins to cholesterol-enriched microdomains. We took advantage of the binding capacity of ganglioside GM1 to cholera toxin subunit B as its membrane receptor for internalization. Ganglioside is concentrated in PM microdomains and excluded from clathrin-coated pits (Nichols 2003), therefore to be considered as a marker for lipid microdomains on cell surface. In hippocampal neurons, the internalized FITC-cholera toxin B with high potassium stimulation co-localizes with DRM marker flotillin 1 (**Figure 4-10** upper panel) and synaptotagmin 1 (**Figure 4-10** lower panel), but not non-DRM marker transferrin receptor. This indicates that at least some of the recycled synaptic vesicle proteins can be retrieved by endocytosis following the same way as GM1 internalization.

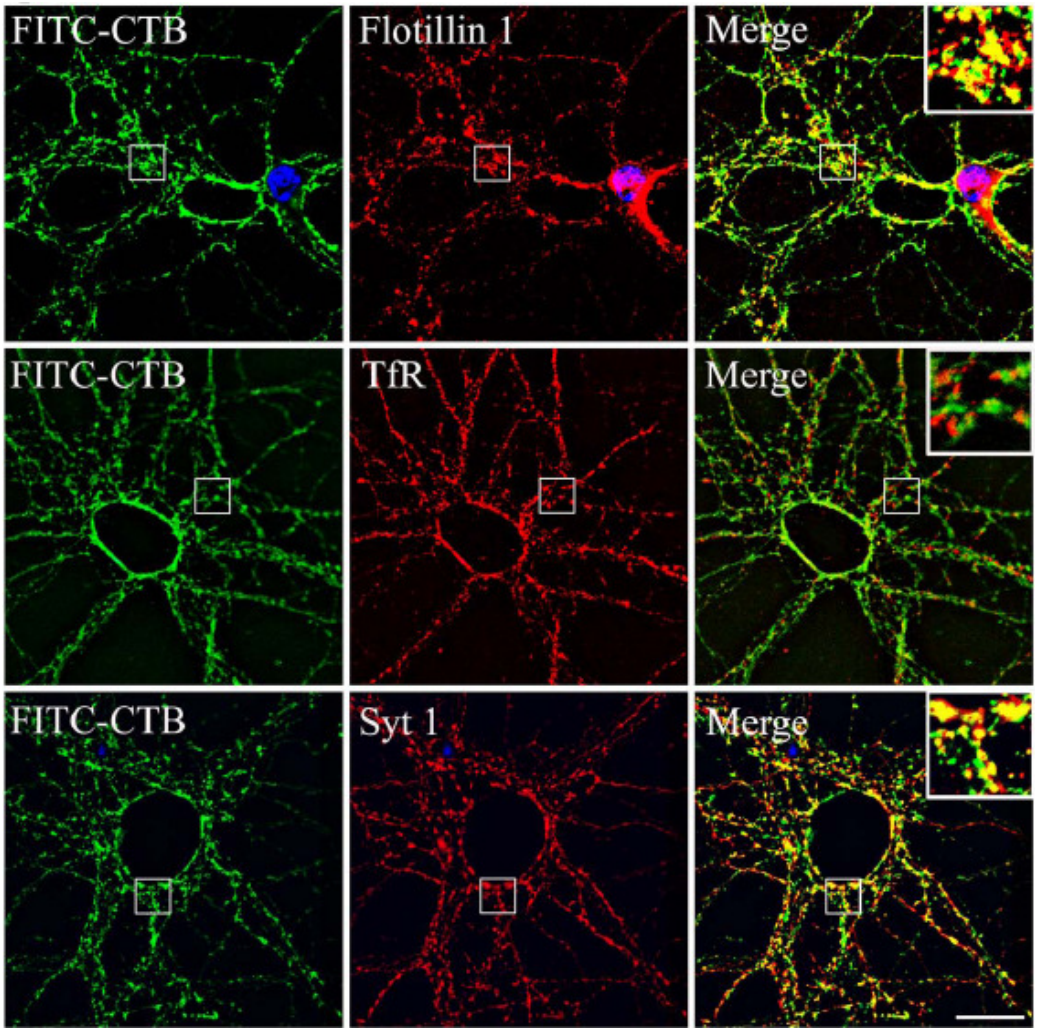

Figure 4-10 Internalized FITC-labelled cholera toxin co-localizes with flotillin 1 and synaptotagmin 1 at synapses

Hippocampal neurons isolated from E18 rats (14 DIV) were washed briefly with Krebs-Ringer-HEPES (KRH) solution and incubated with 10 µg/ml of FITC-CTB in KRH/high K^+ at 37°C for 5 min. Samples were thoroughly washed (3x) with cold KRH solution on ice, fixed and analyzed by indirect immunofluorescence deconvolution microscopy using antibodies against flotillin 1, transferrin receptor (TfR), or synaptotagmin 1 (Syt1). Boxed areas are magnified in the upper-right corner of the merged images. Scale bar, 20 µm.

4.2 Results 2

The second step of coated vesicle transport after cargo enrichment at donor membranes is to initiate membrane curvature. In CME, epsin, amphiphysin and endophilin may operate sequentially or simultaneously to deform the PM. In the case of COP-coated vesicles, the small GTPase Sar1 can insert its NH_2-terminal hydrophobic residue side chains into one layer of the membrane bilayer to help membrane curvature formation. However, the molecular mechanisms of clathrin- and COPI-coated vesicle membrane curvature at the Golgi apparatus are still unknown.

Arfs contain an NH_2-terminal amphipathic helix which is reminiscent of the similar secondary structure in epsin and Sar1. One of the two most intensively studied Arfs, Arf1, can recruit adaptor proteins such as βCOP, AP-1 and GGA for COPI- and clathrin- mediated vesicle transport to the Golgi apparatus. We therefore postulate that Arfs may generally deform their cognate membranes and that Arf1 may facilitate the early step of membrane curvature besides its well-established role to recruit adaptors in clathrin- and COPI-coated vesicle formation.

4.2.1 Characterization of the amino-terminal alpha helix of Arfs

Our secondary structure prediction analysis showed that all six members of the Arf family proteins contain an amino-terminal helix structure with different length as shown in **Figure 4-11 A**. Multiple sequence alignments of the amino-terminal helices (1-14 residue) from all six mammalian Arfs (human does not have Arf2, therefore the Arf2 sequence from rat was used) showed that in addition to the highly conserved Gly2 involved in myristoylation, Leu8 (Ile in Arf6) and Phe9 are well conserved hydrophobic residues. Somewhat less wellconserved amino acids are present at positions 4 and 5 (**Figure 1-1 B**).

The amino-terminal helix is believed to undergo a rotational movement upon GDP to GTP exchange catalyzed by GEF proteins on target membranes. This conformational change not only confers the ability of the flipped amino-terminal helix and modified myristate to interact with the target membrane but also to facilitate the interaction of effector proteins with the inter-loop region between switch I and II.

One interesting feature of the amino-terminal helix within all mammalian Arfs is their amphipathic character (D'Souza-Schorey and Chavrier 2006). Helical wheel analyses are

shown in **Figure 4-12**. All Arfs display a conserved face of yellow colored amino acids in **Figure 4-12**, whereas the opposite side of the helix is occupied by hydrophilic residues including basic charged amino acids in the case of Arf 1-3 and 6. These different properties may contribute to their binding to target organelle membranes and to their biological function.

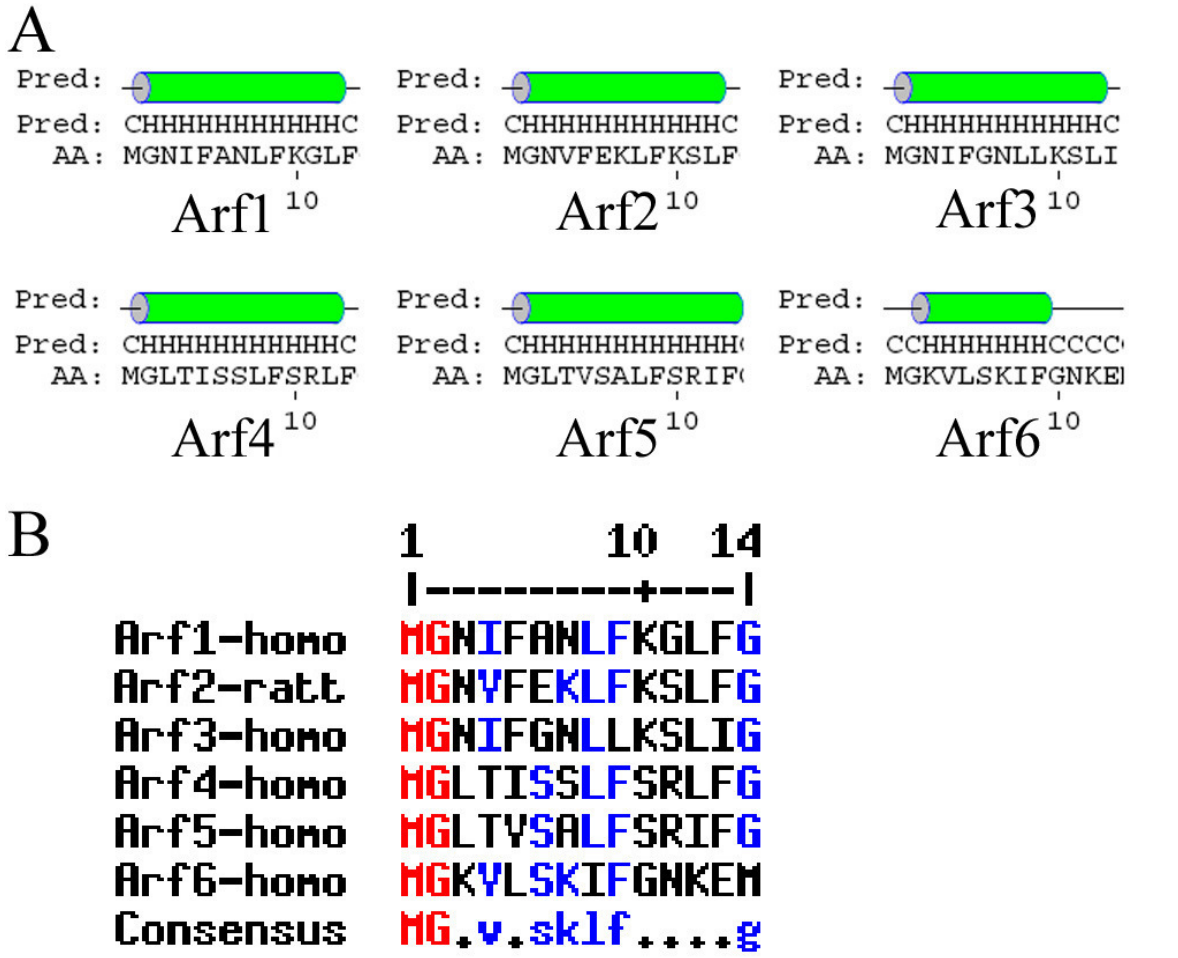

Figure 4-11 Sequence analysis of Arfs

(A) All six mammalian Arfs were subjected to secondary structure analysis using the PSIPRED program and the amino-terminal helices are shown here. Except of the shortest (Arf6 with 9 amino acids) and the longest helix (Arf5 with 13 amino acids), the helices from the other four Arfs contain 12 amino acids. C=coil-coiled and H=helix. (B) Alignment of the first 14 amino acids of mammalian Arfs, red for high consensus, blue for low consensus and black for neutral.

The amino-terminal amphipathic helix found in Arf proteins is contained in epsin and Sar1, two proteins involved in membrane defomation during coated-vesicle traffic. In the case of epsin and Sar1, their amino-terminal helices can deform flat membranes by inserting the side chains of hydrophobic residues found on one side of the helices into one leaflet of the membrane bilayer (Ford, Mills et al. 2002; Lee, Orci et al. 2005). Since Arfs are involved in the initial stages of coat and adaptor protein recruitment in clathrin- and COPI-coated vesicle maturation, we asked whether Arfs could also deform membranes. To study whether Arfs can

bind to liposomes or tubulate liposomes, we established *in vitro* liposome binding and tubulation assays.

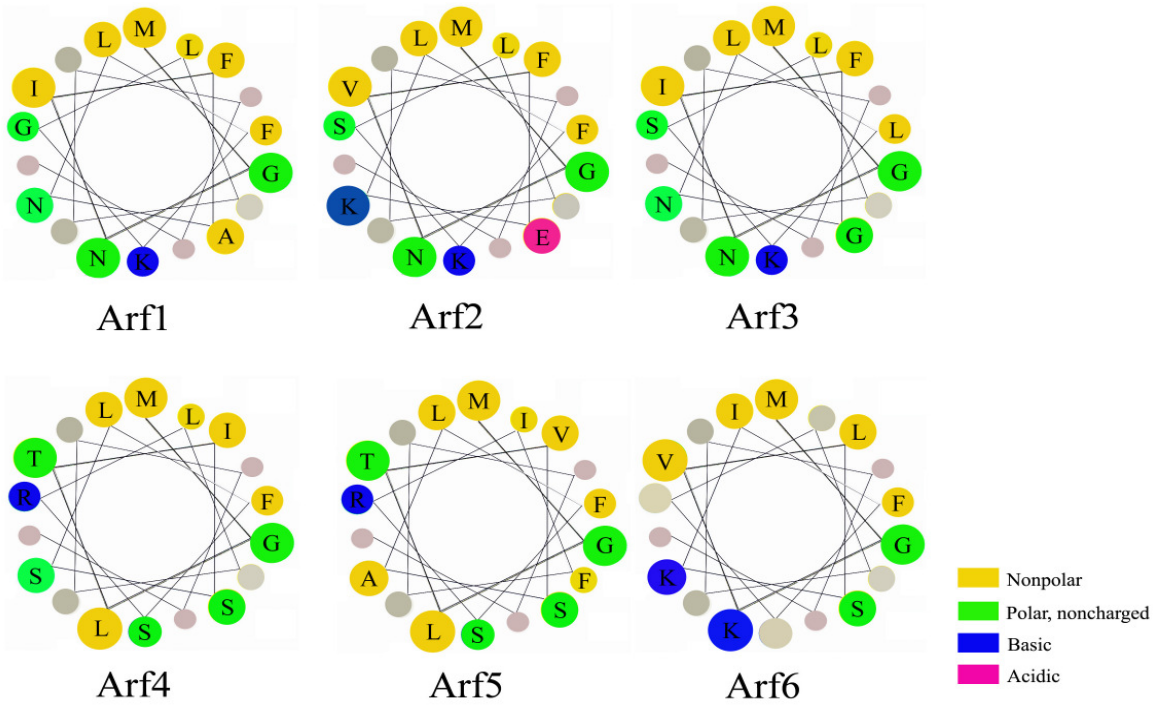

Figure 4-12 Helical wheel analyses of Arfs' amino-terminal helices

Amino-terminal helices of six Arfs were analyzed using the Helical-wheel online program (see methods). Properties of the amino acids are highlighted by different colors. Although all Arf proteins show general amphipathic helical character, they differ in the length of the hydrophobic side and the property of the hydrophilic side.

4.2.2 Profiling of *in vitro* lipid binding of Arfs

To check membrane association of two representative members of the Arf family, Arf1 and Arf6, we performed *in vitro* liposome pull-down assays. Myristoylated Arf1 and Arf6 were expressed in *E.coli* strain ER2566 which was co-transformed with pBB131, a plasmid encoding for yeast *N*-myristoyltransferase (Duronio, Jackson-Machelski et al. 1990). Purified proteins were incubated with liposomes of defined lipid composition at room temperature (RT) for 10 min and then isolated by centrifugation. Proteins that bind to liposomes will be found in the pellet together with liposomes, whereas proteins that do not bind to liposomes stay in the supernatant. As shown in the upper panel of **Figure 4-13**, myristoylated Arf1 binds only to PI(4,5)P_2-containing liposomes. This is somewhat surprising, given that Arf1 is localized to the TGN where PI(4)P is supposed to be the predominant phosphoinositide. Since only a fraction of recombinant Arfs produced in bacteria is N-myristoylated (efficiency ~40%) we were interested in the membrane-binding behavior of non-myristoylated Arfs.

Non-myristoylated Arf1 was purified and binding experiments similar to the ones described above were performed. The middle panel of **Figure 4-13** shows that non-myristoylated Arf1 also specifically binds to only $PI(4,5)P_2$.

In contrast to Arf1, which specifically binds to $PI(4,5)P_2$, we found that both myristoylated and non-myristoylated Arf6 binds to a broad spectrum of negatively charged lipids (**Figure 4-13**). This may reflect the fact that Arf6, different from other Arfs, has a quite basic pI of 8-9 resulting in pronounced electrostatic interactions with negatively charged phospholipids head groups which confers less selectivity for certain lipids at membrane. Since myristoylation is not necessary for liposome binding, non-myristoylated proteins were used for further analysis.

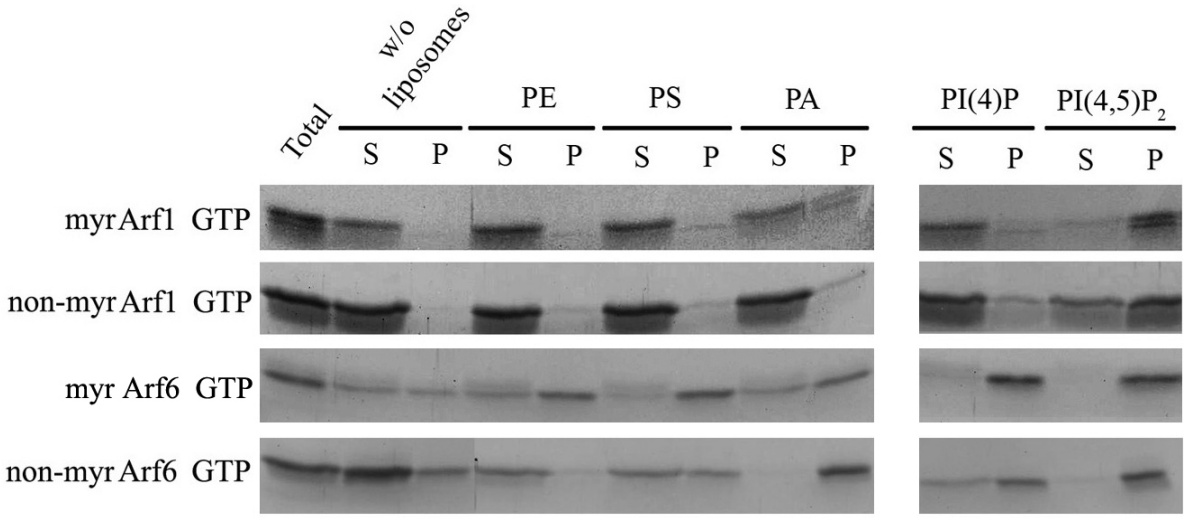

Figure 4-13 Arf1 and Arf6 differ in lipid binding specificity

Liposomes were prepared with 90% PC (phosphatidylcholine), 20% PE (phosphatidyliethanolamine) and 10% of indicated lipid. PA (phosphatidic acid), PI(4)P (phosphatidylinositol 4-monophosphate), $PI(4,5)P_2$ (phosphatidylinositol (4,5)-bisphosphate). LUVs (large unilamillar vesicles) were generated by passing liposomes through 400 nm of polycarbonate membrane. 100 µl of 1 mg/ml liposomes were incubated with 4 µg of myristoylated Arf1, non-myristoylated Arf1 and Arf6 in the presence of 100 µM GTP at RT for 10 min and then centrifuged. Proteins bound to liposomes are shown by Coomassie Blue staining in the bottom fraction. Proteins without liposomes and ENTH that specifically binds $PI(4,5)P_2$ were used as negative and positive controls, respectively. As shown in the figure, non-myristorylated Arf1 binds exclusively to $PI(4,5)P_2$ comparable to the myristoylated Arf1. By contrast, Arf6 binds to a wide range of negatively charged lipids. Total indicates 100% of starting input materials. S, supernatant; P, pellet.

Arfs undergo a cycle of GTP- and GDP-induced conformational changes which determines whether they are localized to membranes or in the cytosol. Based on the known crystal structures, GTP- and GDP-locked mutants were generated for both Arf1 and Arf6. Unexpected to us, our liposome binding assays show that both GTP- and GDP-locked Arf1 and Arf6 bind to membranes as shown by $PI(4,5)P_2$-liposome binding (**Figure 4-14**). This

may either reflect a specific binding to certain lipids or mere electrostatic interactions between the positively charged GTPase-fold and lipid head groups in this *in vitro* system. This is supported by the observation from the crystal structure of Arf1 in its GDP-bound conformation that a patch of basic amino acids is present on the surface of the GTPase between the switch I and switch II regions. The GDP-locked Arf6 mutant also bound to membranes consistent with the observation that overexpressed GDP-locked Arf6 was mainly membrane-localized in fibroblasts (Cavenagh, Whitney et al. 1996; Song, Khachikian et al. 1998).

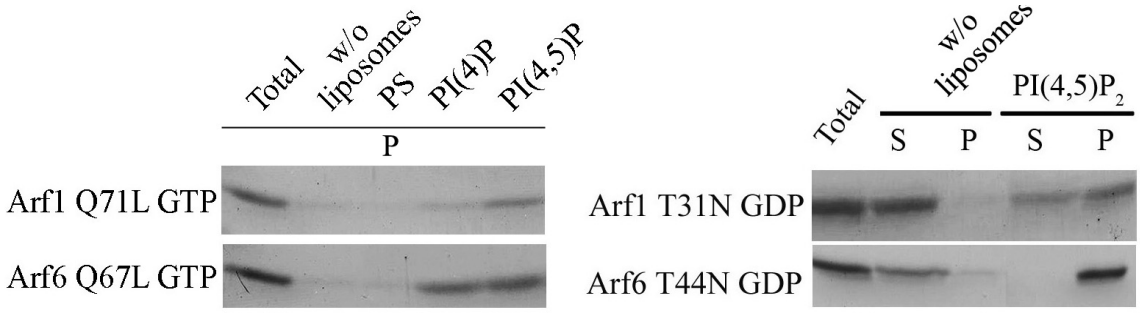

Figure 4-14 GTP- and GDP-locked Arf1 and Arf6 mutants bind PI(4,5)P_2 liposomes

The same experimental procedures were used as for the wild type protein binding assay. Well-characterized GTP- and GDP-locked mutants for Arf6 and Arf1, respectively still bound to liposomes comparable to the wild type proteins.

As shown in **Figure 4-11 B**, residues four, five, eight and nine within the amino-terminal amphipathic helices of Arf 1 and 6 are hydrophobic. A helical wheel analysis shows that these non-polar amino acids are localized on one side of the predicated helix where they are supposed to interact with the membrane. To check whether these hydrophobic residues are important for membrane binding, we selected two combinations of double point mutations from hydrophobic to hydrophilic residues. As seen in **Figure 4-15 A**, combined mutation of residues four and five does not abolish liposome binding of either Arf1 or Arf6; in contrast, mutating residues eight and nine abolishes liposome binding. Since residues eight and nine display higher sequence conservation than residues four and five, the former two may exhibit a larger contribution to the overall membrane binding of Arfs. The specific binding of Arf1 to PI(4,5)P_2 suggests that the head groups of phosphoinositides engage in binding.

Charged cognate residues within the Arf1 helical wheel projection also showed that hydrophilic faces of the predicated amphipathic Arf helices contain different numbers of basic residues which may bind to the head group of phosphoinositides by electrostatic interactions. To address the importance of these basic side chains, we mutated two or three

lysine residues to non-charged residues within or adjacent to the amphipathic helices of Arf1 and Arf6. Liposome binding assays showed that these mutations almost completely disrupted the ability of Arf1 and Arf6 to associate with PI(4,5)P_2-containing liposomes (**Figure 4-15 B**).

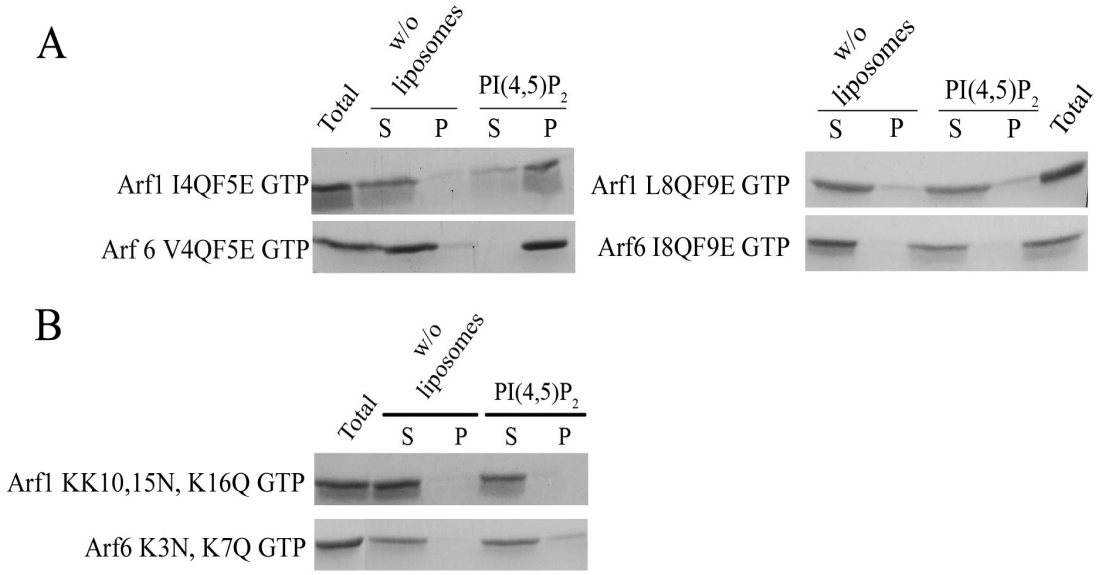

Figure 4-15 Arf1 and Arf6 amino-terminal basic residues are required for liposome binding

(A) Mutation of the hydrophobic residues at the 4th and 5th position to hydrophilic residues of the first ring in the amino-terminal helices of Arf1 and Arf6 do not affect their binding to liposomes; in contrast, similar mutations of the second ring of the helices at residues eight and nine decrease their binding capacity to liposomes dramatically. (B) Mutations of lysine residues on the hydrophilic side of the amino-terminal helices of both Arf1 and Arf6 abolish their binding to liposomes.

4.2.3 Arf1 and Arf6 can deform PI(4,5)P_2-containing liposomes

Insertion of hydrophobic amino acid side chains will promote asymmetry in the membrane bilayer, which results in generation of curvature. Similar mechanisms have been described for epsin (Ford, Mills et al. 2002) and Sar1 (Lee, Orci et al. 2005) in the processes of clathrin-mediated endocytosis and COPII-mediated anterograde transport from ER to Golgi, respectively. Arfs may use a similar mechanism to produce membrane curvature. Based on our liposome binding data, we set out to analyze membrane bending effects on liposomes by electron microscropy (EM). Wild type Arf1 or Arf6 was mixed with PI(4,5)P_2-containing liposomes, applied to a carbon-coated grid, stained with the contrasting reagent uranyl acetate and finally analyzed by EM. Myristoylated Arf1 in the presence of GTPγS generated long tubes with a diameter between 20 to 50 nm. Non-myristoylated Arf1 and Arf6, in the presence of GTPγS, like myristoylated Arf1 tubulated liposomes suggesting that myristoyl modification is not required for liposome binding (**Figure 4-13**) or tubulation (**Figure 4-16**).

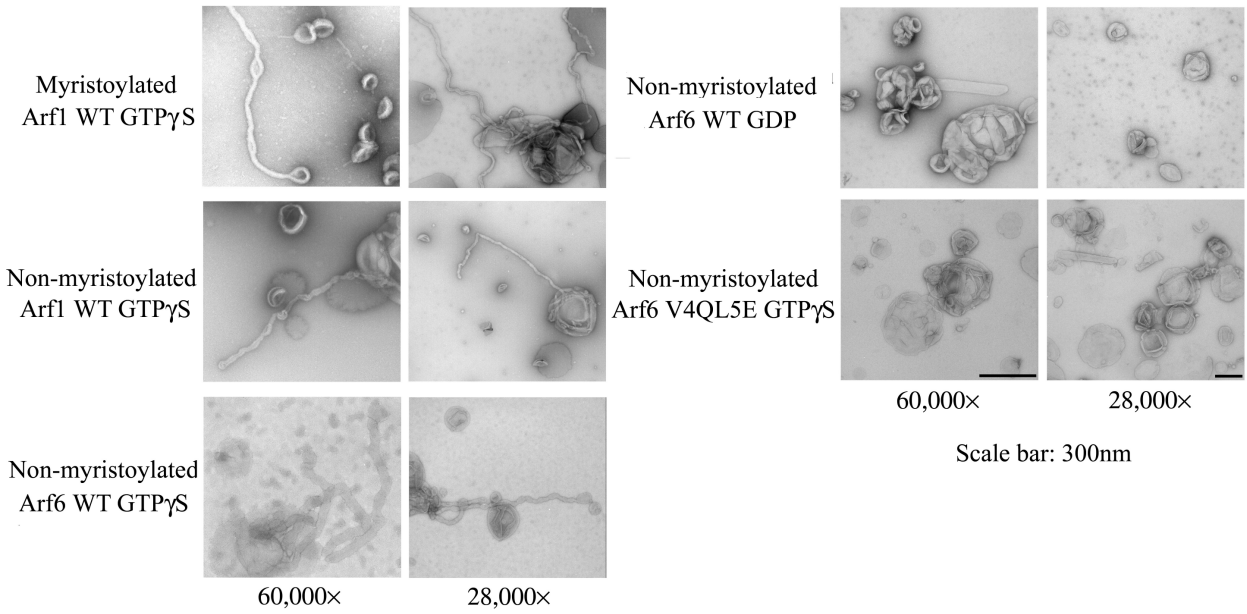

Figure 4-16 Arf1 and Arf6 can tubulate liposomes *in vitro*

Indicated proteins were incubated with PI(4,5)P_2 liposomes for 1 min and then loaded onto the carbon-grid for negative staining. Samples were analyzed by EM. Myristoylated, non-myristoylated Arf1 and non-myrstoylated Arf6 can tubulate round lipsosomes into long tubes in the presence of GTPγS. Arf6 amphipathic helix mutant V4QF5E does not tubulate liposomes even in the presence of GTPγS, only round liposomes can be seen. Non-myristoylated wild type (WT) Arf6 cannot tubulate liposomes in the presence of GDP. Two magnifications of 60,000 and 28,000 were used. Scale bar: 300 nm.

The Arf amphipathic helix flips back to the Arf core structure in the GDP-bound state. Thus, Arf-GDP can not insert its amphipathic helix into the lipid bilayer and induce membrane bending, although Arf-GDP is able to bind to liposomes *in vitro*. Consistent with this, non-myristoylated Arf6 does not tubulate liposomes in the presence of GDP (**Figure 4-16**). An Arf6 mutant in which two of the hydrophobic residues within the NH_2-terminal helix have been exchanged to hydrophilic ones associates with liposomes (**Figure 4-15 A**) but loses its ability to tubulate liposomes *in vitro* (**Figure 4-15**). These data indicate that hydrophobic residues are critical for membrane bending.

Using a second method to validate the tubulation capacity of Arfs, we performed an *in vitro* tubulation assay from lipid membrane sheets. The experimental setup is shown in **Figure 3-2**. As shown in **Figure 4-17**, Arf1 wt can tubulate membrane sheets into tubular structures, whereas Rab11 wt and two Arf1 NH_2-terminal hydrophobic mutants, I4Q and I4Q/F5E, do not change lipid membrane sheet morphology dramatically.

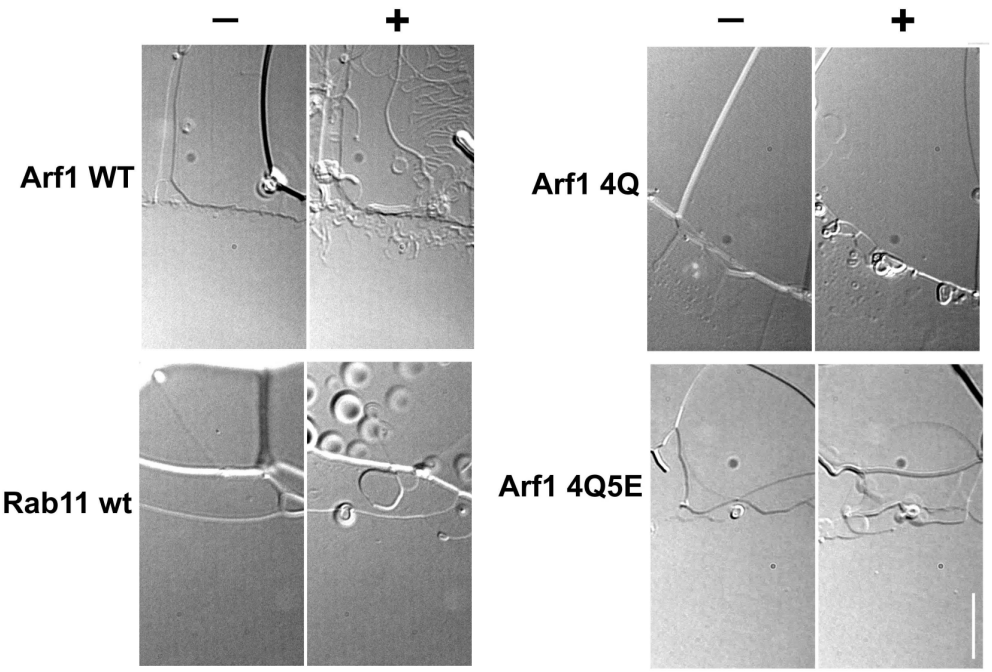

Figure 4-17 Arf1 wt but not Rab11 wt and Arf1 NH_2-terminal hydrophobic mutants tubulate lipid membrane sheets *in vitro*

Experimental procedures are described in Materials and Methods. Lipid membrane sheet edges where injected proteins migrate towards are shown here. Arf1 wt in the presence of GTP can tubulate lipid membrane sheets. Arf1 NH_2-terminal hydrophobic mutants, I4Q and I4Q/F5E, and another small GTPase Rab11 only cause lipid membrane sheet expansions (In collaboration with Dr. Aurelien Roux). Scale bar: 10 μm.

One interesting phenomenon was observed when we modified our protocol to mix pre-sedimented liposomes with non-myristoylated Arf6 on the carbon-grid for EM. In addition to the tubular structures, many buds formed on the end of the tubes and protein coated small vesicles could be observed. These structures were not seen in the experiments employing a pre-mix protocol. One can imagine that the pre-sedimented liposomes may be temporally attached to the grid; the twisting tension resulting from the added Arfs to bend membranes between two ends may create longitudinal tension that leads to fission as in the case of dynamin (Roux, Uyhazi et al. 2006). Since GTPγS was used in this experiment, we do not know whether this phenomenon is a new mechanism or just an *in vitro* artefact. Further evidence is needed for clarification.

4.2.4 *In vivo* characterization of Arf1 and its mutants

Endogenous Arf1 mainly localizes to the peri-nuclear region (**Figure 4-18** left) and recruits adaptor proteins such as AP-1, GGA1 or βCOP to facilitate clathrin- or COPI-coated vesicle formation. Arf1 itself is recruited to the membrane by at least three mechanisms that include GEF-mediated nucleotide exchange (Tsai, Adamik et al. 1993), phosphoinositides (Ge, Cohen et al. 2001), and myristoyl modification. Although PI(4,5)P_2 is sufficient for Arf1

membrane recruitment *in vitro*, GEF is required for its membrane recruitment *in vivo*. This view is supported by the activity of BFA which disrupts the peri-nuclear localization of Arf1 and its effector proteins. Hydrophobic side chains of the amphipathic helix can contribute extra force to stabilize Arf1 membrane attachment (Antonny, Beraud-Dufour et al. 1997; Losonczi and Prestegard 1998; Seidel, Amor et al. 2004; Harroun, Bradshaw et al. 2005) which is consistent with our data presented here. This may be a prerequisite for membrane bending. Overexpressed Arf1 mutated in the second glycine residue (G2A) did not co-localize with the TGN marker AP-1 in COS7 cells, but remained cytosolic (**Figure 4-18**). This demonstrates the importance of myristoyl modification for correct membrane targeting of Arf1 *in vivo* and indicates that it is a critical factor for membrane recruitment. This stabilization effect may contribute to the anchoring of Arf1 long enough to fulfill the function in its active conformation.

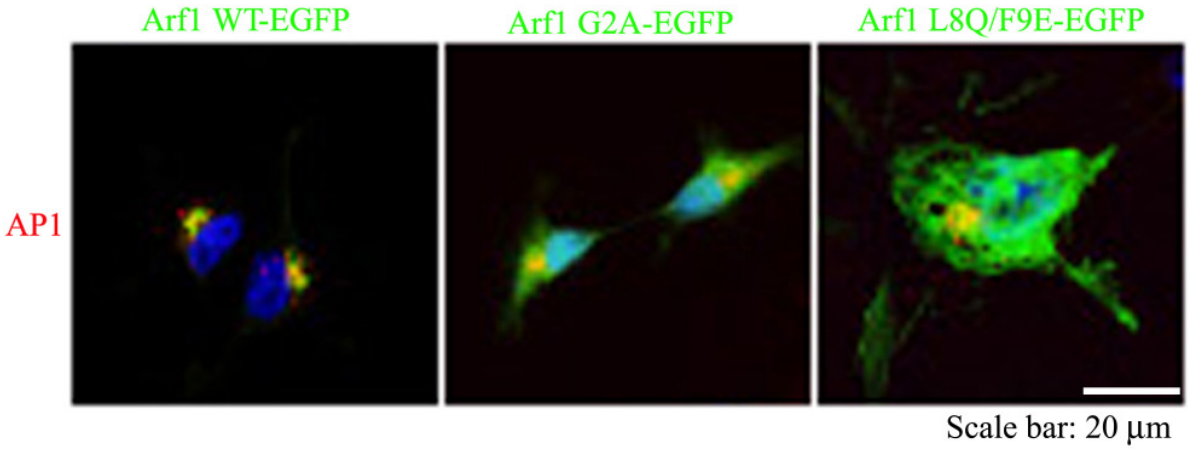

Figure 4-18 Non-myristoylated and hydrophobic mutants of Arf1 abolish their peri-nuclear location in COS7 cells

COS7 cells were transfected with EGFP-tagged Arf1 WT and corresponding mutants as indicated in the figure. After plating onto coverslips, cells were fixed and incubated with specific monoclonal antibody against AP-1 followed by a secondary antibody labeled with Alexa 594 for visualization. In the left column, wild type Arf1-EGFP co-localizes with AP-1 in the peri-nuclear regions. Overexpressed myristoylation mutant protein, Arf1-G2A-EGFP, showes a dispersed cytosolic distribution. Arf1 amino-terminal hydrophobic mutant, L8QF9E, also dissociates from the peri-nuclear region and does not co-localize with AP-1. Scale bar: 20 µm.

Mutation of the hydrophobic face of its amphipathic helix resulted in a mutant of Arf1 (I8QF9E) that shows a cytosolic distribution upon overexpression in COS7 cells and in this case Arf1 does not co-localize with AP-1 (**Figure 4-18**). This may be caused either by lost membrane stabilization and further membrane bending or simply a disruption of myristoyl modification. Further biochemical experiments are needed to confirm whether this mutant is correctly myristoylated. In this case, the amino-terminal hydrophobic residue side chain insertion into the membrane and subsequent curvature generation are important for the normal localization and function of Arf1.

To test whether Arf1 can deform membranes *in vivo*, Carboxy-terminal EGFP-tagged Arf1 WT was overexpressed in COS7 cells. Live cell imaging was used to monitor structures where Arf1 localized. Still images from different time points were selected and shown in **Figure 4-19**. Arf1-EGFP decorates mobile and dynamic tubular structures emanating from the perinuclear region as indicated by the arrowheads.

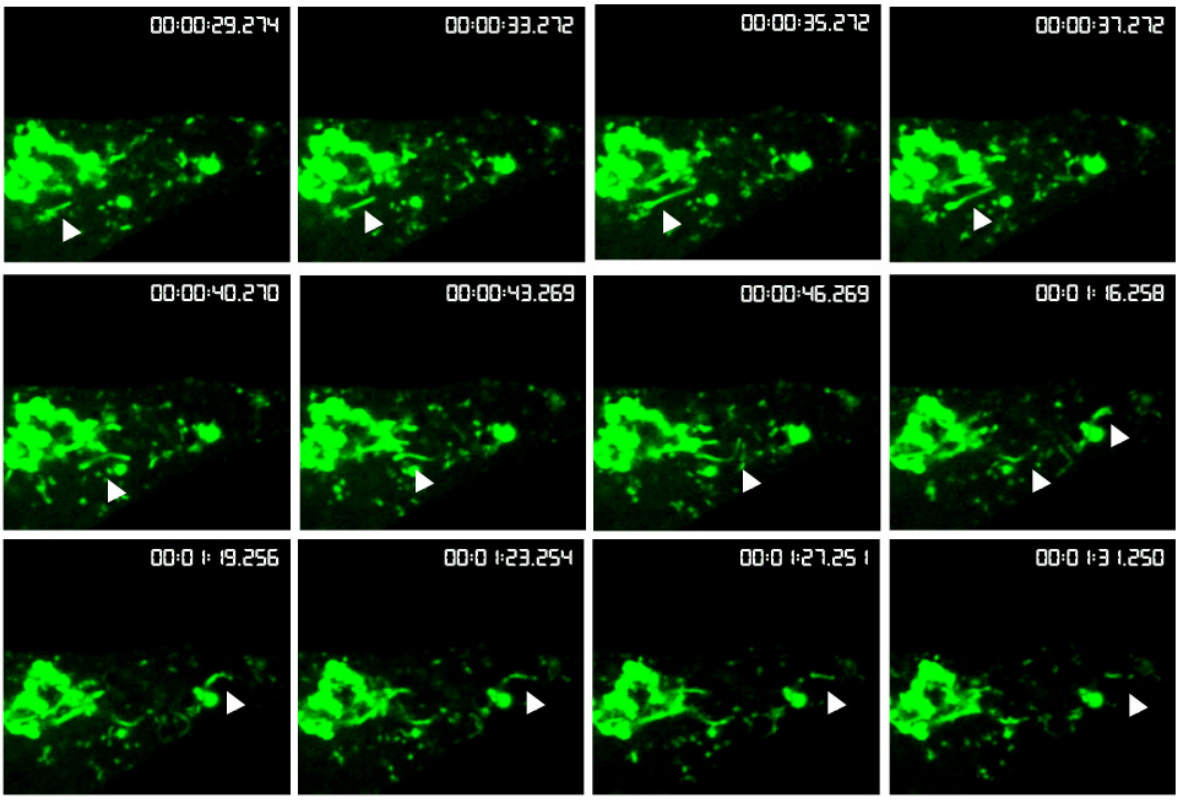

Figure 4-19 Overexpressed Arf1-EGFP decorates tubular structures in COS7 cells

Arf1-EGFP was transfected in COS7 cells for 8 h. After splitting on to glass chambers for overnight, cells were monitored by spinning disk microscope in the GFP channels for 5 min. Still images were selected as the indicated time points. (From Michael Krauss)

Although overexpressed Arf1-EGFP decorates the tubular structures in perinuclear regions, we can not exclude the possibility that Arf1-EGFP just localizes to the tubules formed by other proteins in the same place. Therefore, NH_2-terminal 24 residues of Arf1 was fused to EGFP and overexpressed in COS7 cells. Massive tubular structures were observed as shown in the upper panel of **Figure 4-20**. In contrast, one mutant with residues four and five mutated to hydrophilic residues lost its membrane localization and was completely cytosolic (**Figure 4-20**, lower panel). These indicate that the Arf1 NH_2-terminal amphipathic helix is sufficient to deform membranes *in vivo* and, the hydrophobic residues in this helix are important for membrane binding and deformation.

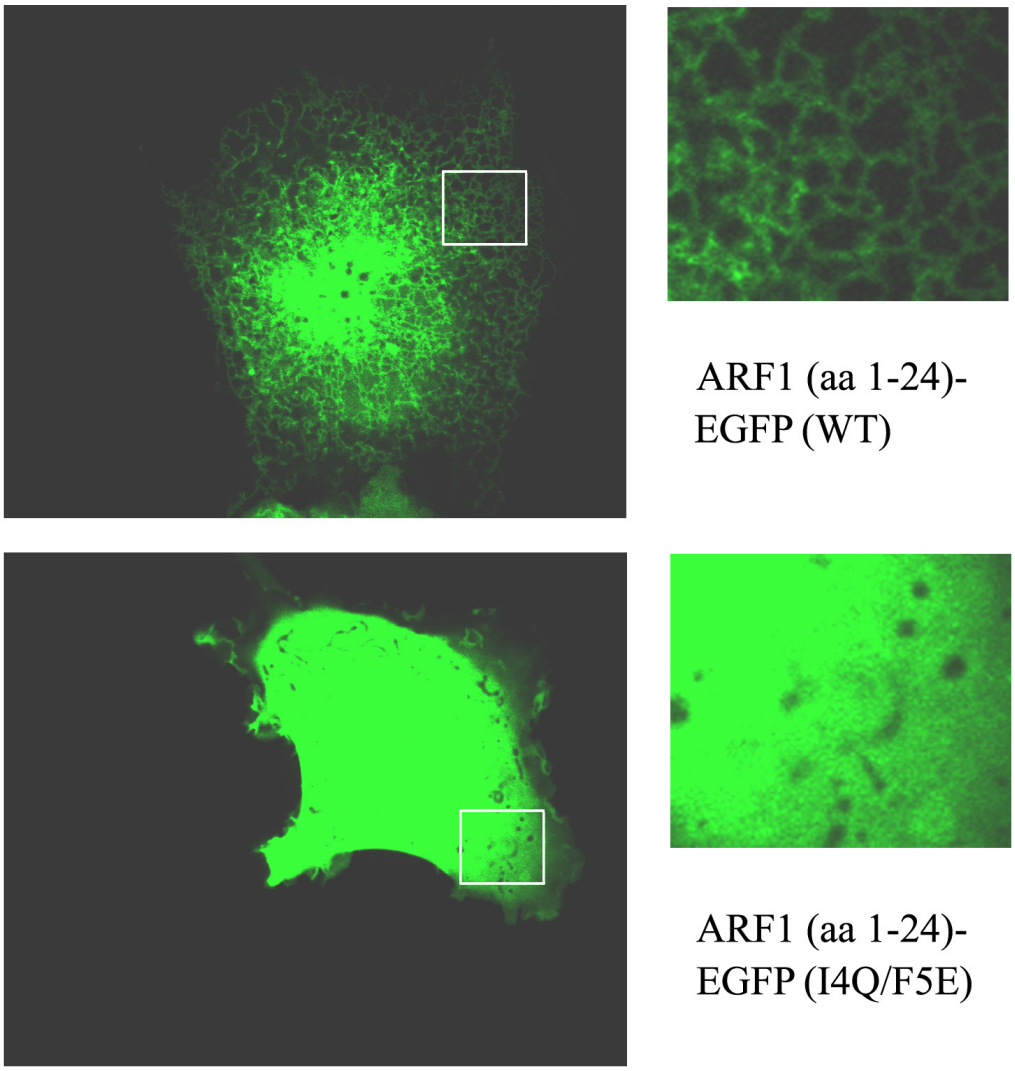

Figure 4-20 NH_2-terminal amphipathic helix of Arf1 but not the hydrophobic mutant produces massive tubules when overexpressed in COS7 cells

Arf1 1-24-EGFP WT and Arf1 1-24-EGFP I4Q/F5E were overexpressed in COS7 cells. Experimental procedures were the same as that of **Figure 4-19**. Four time enlarged images of the indicated box areas from the left side images are shown in the right side. (From Michael Krauss).

4.2.5 Establishment of an *in vitro* minimal system for membrane budding

Tubes generated by the amphipathic helix insertion are not very stable as observed by live-imaging of flat lipid membrane sheets *in vitro*. Arfs are among the initial factors recruited to membranes during adaptor and coat protein-mediated vesicle formation. It is thus possible that membrane deformation may be further stabilized by coat proteins that have intrinsic curvature. Consistent with this idea, a recent study reported that epsin localized on flat inner membrane leaflets when clathrin was knocked down by RNAi (Hinrichsen, Meyerholz et al. 2006). We thus tried to establish a minimal *in vitro* system to study Arf1-dependent budding of clathrin-coated vesicles.

To answer the question of whether adaptors and coat proteins can stabilize tubules generated by Arfs, we chose Arf1 its downstream adaptor GGA1 and clathrin to study their role in the process of membrane curvature and coated vesicle budding *in vitro*.

The domain structure of GGA1 is shown in **Figure 1-5**. Both full length GGA1 and GGA1Δ1-426 were constructed by fusion with an NH_2-terminal His_6×tag. Recombinant proteins were expressed in *E.coli* and purified by Nickel Affinity Gel (**Figure 4-21**).

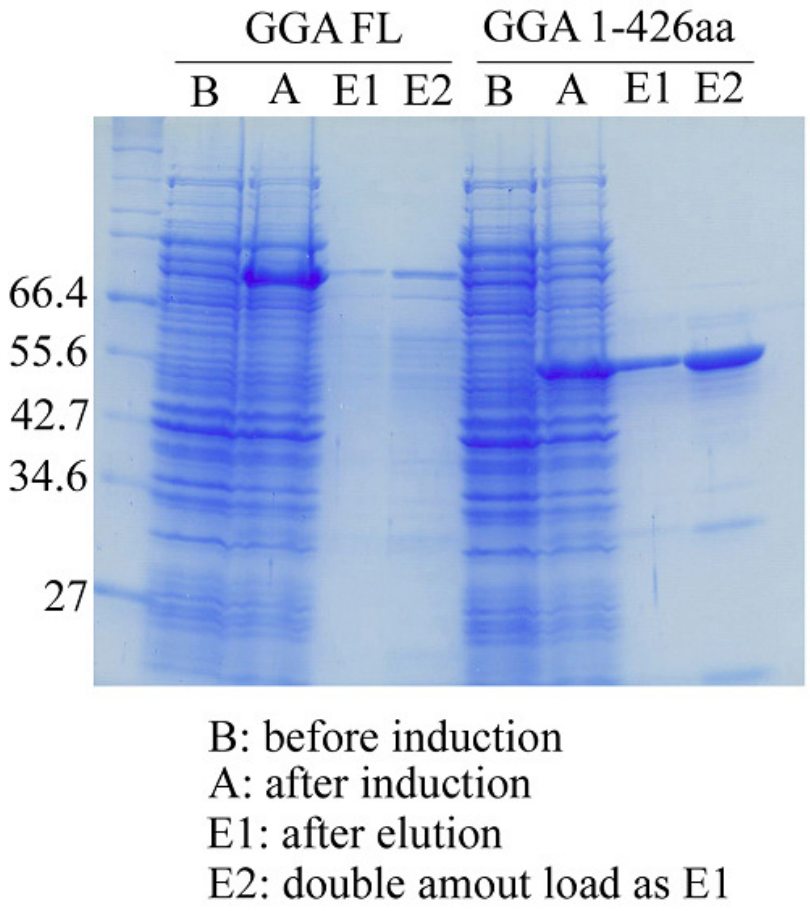

Figure 4-21 Affinity purification of GGA1

Mouse GGA1 full length and 1-426 amino acids NH_2-terminal truncated cDNA sequences were inserted into pET28a vector. Proteins expression was induced with 0.5 mM IPTG at 30°C for 4 h. Cells were broken by lysozyme, sonification and detergent. Cell lysates were incubated with Nickel beads at 4°C for 1.5 h. After 3× washing, proteins were eluted with 1.5 ml of elution buffer in the presence of 200 mM of imidazole. 5 µl and 10 µl of elution samples were used in lane E1 and E2, respectively. The expression and purification of the proteins were analyzed by SDS-PAGE and stained with Coomassie Blue.

The GGA1Δ1-426 protein sequence stops one residue after the putative clathrin box in the second linker region between the GAT and GAE domains as shown in **Figure 1-5**. After one-step affinity purification using Nickel beads, we got better purity of His_6×tagged-GGA1Δ1-426 protein than for the His_6×tag full length GGA1 (**Figure 4-22**). Therefore, we chose His_6×tag-GGA1Δ1-426 for further studies.

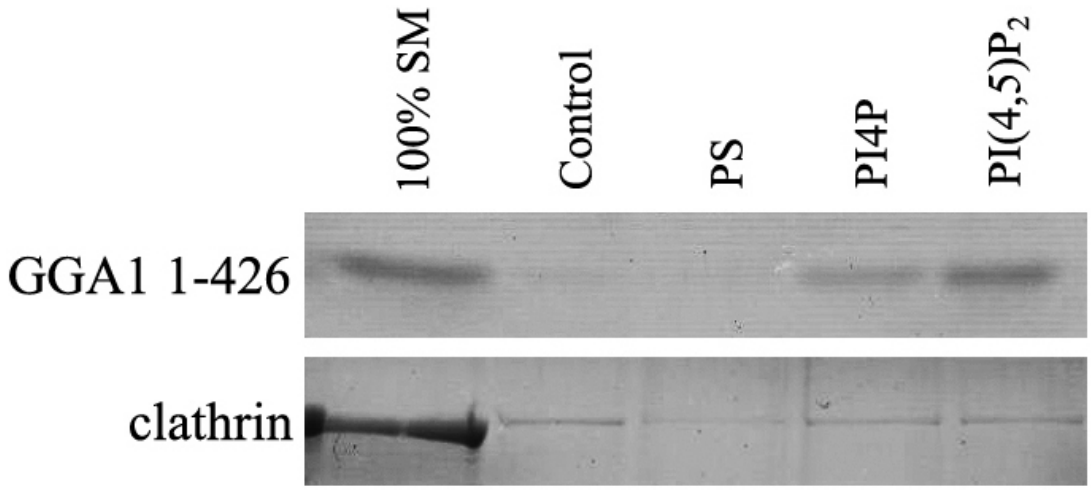

Figure 4-22 His_6×tagged-GGA1Δ1-426 and clathrin liposome binding assays

The same protocol was used as described in **Figure 4-13**. A truncated His_6×tag-GGA1 containing VHS, GAT and clathrin box His_6×tag-GGA1Δ1-426 and clathrin purified from pig brain were used. Only the pellet signals are shown here.

The truncated human His_6×tag-GGA1Δ1-426 that contains a VHS, GAT domain and the clathrin box in the unstructured second linker region can bind PI(4)P- and PI(4,5)P_2-liposomes *in vitro*, but cannot tubulate lipid membrane sheets. Clathrin does not bind liposomes at all.

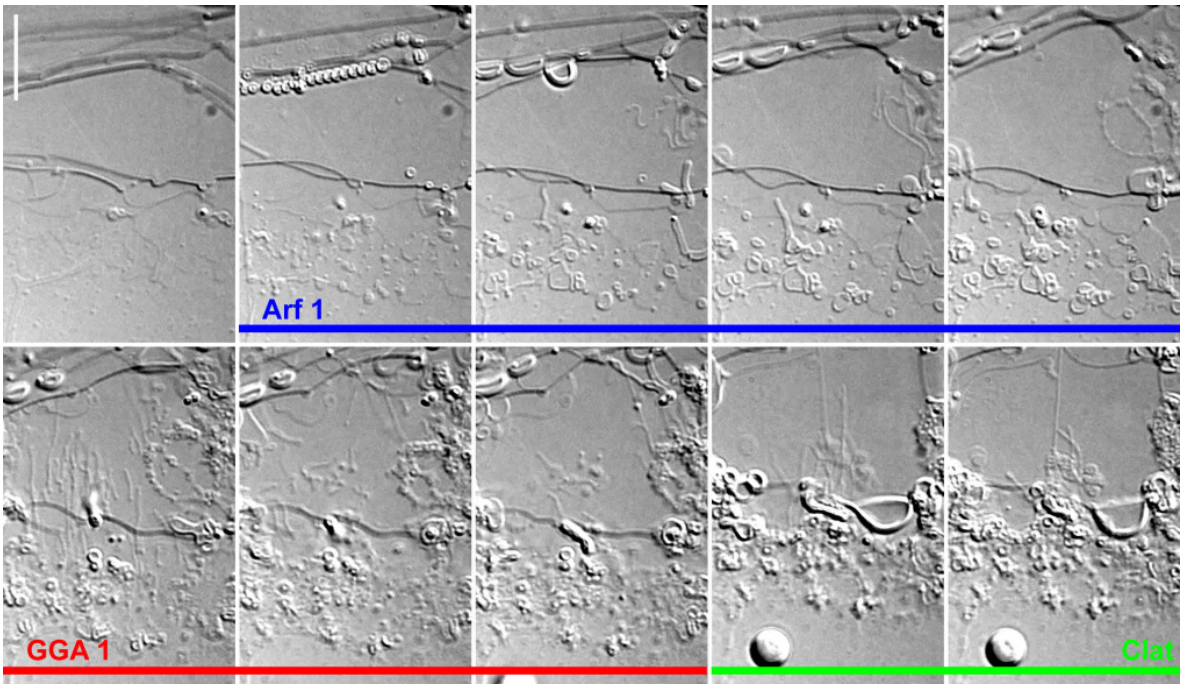

Figure 4-23 Generation of clathrin-coated buds *in vitro*

The experimental setup is illustrated in **Figure 3-2**. Arf1 WT was injected first in the presence of GTP followed by immediate loading with His_6×tag-GGA1Δ1-426 and clathrin. Morphological changes of lipid membrane sheets were observed with the DIC (differential interference contrast) model in live time. Green color indicates the injection of clathrin (In collaboration with Dr. Aurelien Roux, Yale University). Scale bar: 10 µm.

We observed that the tubules generated by Arf1 alone from lipid membrane sheets were unstable and retract quickly after formation. When His_6×tag-GGA1Δ1-426 and clathrin were sequentially added after Arf1 application to the lipid membrane sheet, long, straight and stable tubules were seen which lasted for 30 min. This straight tubular structure is very similar to the tubes formed by F-BAR proteins (Itoh, Erdmann et al. 2005) and dynamin (Roux, Uyhazi et al. 2006), which points to a possible polymerization mechanism during membrane deformation. Interestingly, the addition of clathrin even triggered the generation of capped tubular ends which are reminiscent of clathrin-coated buds *in vivo* (**Figure 4-23**).